JOURNAL OF THERMOPHYSICS AND HEAT TRANSFER
Vol. 9, No. 1, January–March 1995

Dependence of Heat Transfer to a Pulsating Stagnation Flow on Pulse Characteristics

E. C. Mladin* and D. A. Zumbrunnen†
Clemson University, Clemson, South Carolina 29634

A detailed boundary-layer model is implemented to ascertain the influence of pulse shape, frequency, and amplitude on instantaneous and time-averaged convective heat transfer in a planar stagnation region formed beneath an incident periodic, pulsating flow with temperature-dependent kinematic viscosity and thermal conductivity. Interactions between low-frequency/high-amplitude flow pulsations and the nonlinearities in the governing equations lead to reductions in time-averaged Nusselt numbers up to 16%. Predictions are in good agreement with experimental results. A means to suppress heat transfer is thus suggested that may have practical application to gas turbines where blades are exposed to a periodic flow. Phase portraits, Poincarè maps, Fourier spectra, and Lyapunov exponents are used to elucidate the most complex solutions.

Nomenclature

C = steady-state freestream velocity gradient
C_t = instantaneous freestream velocity gradient
C_* = constant dimensionless freestream velocity gradient from potential flow theory, $C_t w/V_i$
c_p = specific heat at constant pressure
d = cylinder diameter
f = frequency of imposed sinusoidal incident flow variation
f_q = frequency of imposed sinusoidal surface heat flux
f_{q*} = dimensionless frequency, f_q/C
f_* = dimensionless frequency, f/C
$f_1, f_2, \ldots, f_5$ = functions defined by Eqs. (26–30)
g = function defined by Eq. (31)
h = heat transfer coefficient
k = thermal conductivity
Nu_w = Nusselt number, hw/k
Nu_* = ratio of instantaneous Nusselt number to steady-state Nusselt number, Nu_w/Nu_{w0}
q_s = surface heat flux
q_{s*} = dimensionless surface heat flux, Eq. (22)
q_{s0*} = dimensionless surface heat flux for $t = 0$ and steady-state conditions, Eq. (38)
Pr = Prandtl number evaluated at T_{film0}
p = instantaneous local static pressure
Re_w = Reynolds number, $V_{i0}w/\nu$
Sr_w = Strouhal number, $fw/V_{i0} = f_*C_*$
T = fluid temperature
T_f = film temperature, $(T_s + T_\infty)/2$
T_s = surface temperature
T_∞ = freestream temperature
t = time
U_∞ = local velocity component parallel to the surface in the freestream
$U_{\infty*}$ = dimensionless freestream velocity, U_∞/V_{i0}
u = local velocity component parallel to the surface and within the hydrodynamic boundary layer
u_* = dimensionless velocity, u/U_∞
V_i = incident flow velocity
V_∞ = local velocity component normal to the surface in the freestream
v = local velocity component perpendicular to the surface and inside the hydrodynamic boundary layer
w = characteristic length scale, jet width or cylinder diameter, also jet diameter in Table 1
x = distance along impingement surface from stagnation line, Fig. 1
x_* = dimensionless distance, x/w
y = distance perpendicular to impingement surface, Fig. 1
α_k = dimensionless coefficient in Eq. (16), $k_f^{-1}(T_{s0} - T_\infty)(\partial k_f/\partial T)\,|\,T_{f0}$
α_ν = dimensionless coefficient in Eq. (15), $\nu_f^{-1}(T_{s0} - T_\infty)(\partial \nu_f/\partial T)\,|\,T_{f0}$
β = dimensionless distance, y/Δ
Γ = dimensionless thermal boundary-layer thickness, $C\Delta^2/\nu_f$
Δ = instantaneous thermal boundary-layer thickness
δ = instantaneous hydrodynamic boundary-layer thickness
ε_1 = dimensionless peak to mean amplitude for periodic flow variation, Eq. (36)
$\varepsilon_2, \varepsilon_3$ = dimensionless peak to mean amplitude for periodic surface heat flux variations, Eqs. (37) and (39)
η = dimensionless distance, y/δ
θ = dimensionless fluid temperature, $(T - T_\infty)/(T_{s0} - T_\infty)$
θ_s = dimensionless surface temperature, $(T_s - T_\infty)/(T_{s0} - T_\infty)$
Λ = dimensionless hydrodynamic boundary-layer thickness, $C\delta^2/\nu_f$
μ = dynamic viscosity
ν = kinematic viscosity, μ/ρ
ξ_1, ξ_2 = dimensionless coefficients in the double-ramp variations, Eqs. (36) and (37)
ρ = mass density
τ = dimensionless time, Ct

Received Dec. 20, 1993; revision received April 28, 1994; accepted for publication April 28, 1994.

*Graduate Research Assistant, Thermal Sciences Research Laboratory, Department of Mechanical Engineering.
†Associate Professor, Thermal Sciences Research Laboratory, Department of Mechanical Engineering. Member AIAA.

Ψ_1–Ψ_4 = functions defined by Eqs. (19–21) and (32)
Ω, Ω_1, Ω_2 = dimensionless variables defined by Eqs. (13), (18a), and (18b)
ω = function defined by Eq. (14)

Subscripts
avg = time-averaged value
f = pertaining to initial film temperature T_{f0}, $(T_{s0} + T_\infty)/2$
0 = pertaining to $t = 0$ and/or steady-state (nonpulsating) conditions

Introduction

RECENTLY, a related study[1] demonstrated that the equations governing the dynamical responses of the hydrodynamic and thermal boundary layers to a pulsating incident stagnation flow are highly nonlinear. Because of nonlinearities, sinusoidal fluctuations in an incident flow can lead to nonsinusoidal variations in dependent variables such as instantaneous convective heat transfer coefficients. Thus, an opportunity to modify heat transfer rates is suggested by the nonlinearities. With this motivation, the influence of the incident velocity waveform (i.e., pulse shape), pulsation frequency, and pulsation amplitude are investigated in this study. Of particular interest is whether convective heat transfer can be enhanced in impinging jet flows or diminished near the leading edge of turbine blades by careful selection and control of the pulse characteristics. Gas turbine blades reside in a periodic flow as they travel past stationary nozzles. If pulsations lead to reduced heat transfer, it may prove feasible to modify designs so as to induce the pulse characteristics that are most effective in reducing heat transfer. Similarly, careful selection of pulse characteristics might make heat transfer enhancement possible in jet flows. Such enhancements would be effective at small Reynolds numbers where turbulence effects are minimal or nonexistent. The influence of temperature-dependent properties and simultaneous variations in a surface heat flux are also considered in this study for completeness. The inclusion of an unsteady heat flux was deemed appropriate since unsteady heat generation may occur in electrically or radiatively heated surfaces, and directly influence the dynamical response of the thermal boundary layer in concert with flow pulsations.

Transient convective heat transfer in stagnation flows has been considered in several studies where the transients are induced by a periodic or impulsive motion in the freestream velocity. Theoretical and experimental works related to this study are summarized in Table 1. Deviations from steady-state Nusselt numbers and the related cause are summarized in the last column. Although many of the tabulated studies revealed no significant effects on time-averaged heat transfer due only to the presence of flow pulsations, it should be noted that limited combinations of major parameters, such as pulse amplitude and frequency, pulse shape, and Prandtl number have been considered. However, several of the more recent experimental studies reported significant changes in the time-averaged Nusselt number within the stagnation region. Thus, an opportunity to affect heat transfer rates in stagnation flows by inducing pulsations has been recently established. These studies are generally characterized by higher Strouhal numbers Sr_w, and higher pulse magnitudes ε_1.

The stagnation region that is considered is depicted in Fig. 1a. Such flows arise beneath impinging planar or "slot" jets, on a cylinder in a crossflow, or in the front stagnation region of any bluff body where the frontal surface can be effectively represented by a tangent plane. Although the incident flow velocities U_∞ and V_∞ may be unsteady, it is assumed that symmetry in the flow is preserved about the stagnation line ($x = 0$). The hydrodynamic and thermal boundary layers thereby remain spatially constant in the vicinity of $x = 0$. Thus, spatial variations that arise as a consequence of asymmetries in the incident flow are not considered. Selected forcing functions for the incident pulsating flow velocity have been selected so that they converge smoothly to the steady flowfield as temporal variations become small. These steady velocity components are given by Schlichting[2] as

$$U_\infty = Cx \tag{1a}$$

$$V_\infty = -Cy \tag{1b}$$

where

$$C = C_* V_i / w \tag{1c}$$

The heat transfer condition at the impingement surface $y = 0$ is specified by the functions $q_s(t)$, while the temperature T_∞ is assumed to remain constant. The dimensionless velocity gradient C_* depends on the flow characteristics and the surface geometry, and can be calculated from potential flow theory or from experimental measurements.[3–5] In the analysis that follows, C_* is found to influence the dimensional transient response significantly. Values for some common stagnation

Table 1 Prior studies related to pulsating stagnation flows

Reference	Type of work	Fluid	Geometry	Re_w	Sr_w	ε_1, %	$Nu_{*,\mathrm{avg}} - 1$, %
16	Experimental	Air	Cylinder in crossflow	60–400	——	≤45	−4.3–0.0
17	Experimental	Air	Cylinder in crossflow	2,500–15,000	≤0.07	≤20	≈0.0
18	Experimental	Air	Circular jet	1,200–12,000	0.0001–0.01	0–100	≈0.0
19	Theoretical	$Pr = 0.72$	Planar stagnation	——	0.7	30	20 (Ts = const)
20	Experimental	Water	Cylinder in crossflow	3,500	0.06–0.18	(0.89–1.99)d	40–60 (wake capture)
21	Experimental	Air	Cylinder in crossflow	50,000	0.0063–0.244	4–25	≈0.0
22	Theoretical	$Pr = 0.7$	Axisymmetric stagnation	0.01–100	0–19	<<1	$f(f_*, \varepsilon_1)$
23	Experimental	Hot exhaust gas	Circular jet	6,630; 9,700	0.5	Flow reversal	≤250 (flow reversal)
24	Experimental	Water	Planar jet	3,100–20,750	0.26–0.365	100	≤100 (boundary-layer renewal)
1	Theoretical	$Pr = 0.7$–15	Planar stagnation	——	0.008–0.4	0–60	−16–2 (nonlinear dynamics)
9	Experimental	Water	Planar jet	3,000–20,000	0.011–0.964	0.5–85	−17–0 (nonlinear dynamics)
						100	≤33 (boundary-layer renewal)

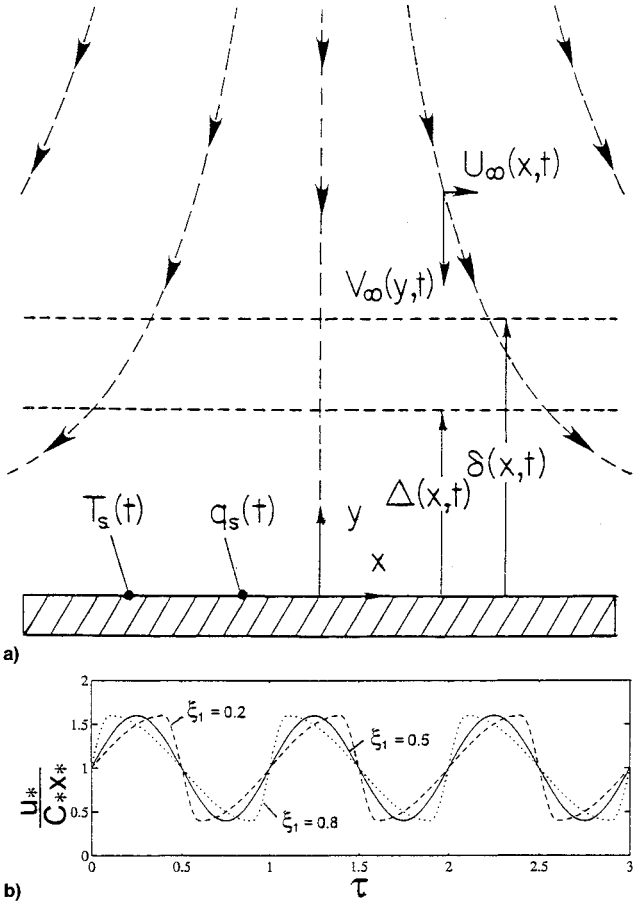

Fig. 1 a) Unsteady planar stagnation flow on a surface with time-dependent heat flux and b) flow pulsations with sinusoidal ($\xi_1 = 0.5$) and ramp-up/ramp-down ($\xi_1 \neq 0.5$) waveforms.

flows have been tabulated[6] and may be used to adapt the dimensionless results of this study to a specific application. Examples of waveforms considered for the incident free-stream flow pulsations are shown in Fig. 1b. A mathematical description of these waveforms is provided later; however, a single function has been developed to represent pure sinusoidal pulsations, ramp pulsations, and pulsations with intermediate waveforms. It should be noted that theoretical and experimental studies have shown that the local heat transfer coefficient is spatially constant to within 1% over a distance equal to about one-half jet width from the stagnation line of a laminar planar jet with a uniform fluid discharge velocity across the nozzle width. This uniformity is attributable to the symmetry of the impinging flow (Fig. 1a) and extends the validity of this study to regions away from the stagnation line.

Analysis

Description of Analytical Method and Assumptions

The responses of nonlinear systems are commonly represented by a reduced system of first-order, ordinary differential equations, in order to make use of many diagnostic tools for evaluating complex and chaotic behaviors, and since transients must be evaluated over long time intervals for different parametric values. Therefore, partial-differential equations for mass, momentum, and energy conservation in the fluid were transformed into ordinary differential equations with the use of some approximations. The approach that was developed is related to the von Karman-Pohlhausen technique. This technique has been widely applied to studies of hydrodynamic boundary layers on airfoils, where the hydrodynamic boundary layer is significantly influenced by a pressure gradient, as in stagnation flows. In the related technique implemented here, equations for momentum and energy conservation in their integral and differential forms are used with temporally adaptive profiles for fluid velocity and temperature to obtain governing equations for the hydrodynamic and thermal boundary-layer responses. However, since the method is well-suited to a stagnation flow, it was deemed more suitable than those commonly used in other nonlinear and chaotic dynamics studies, such as methods employing truncated perturbation series or limited basis functions in Galerkin or spectral techniques. As will be demonstrated later, the technique has yielded predictions in very good agreement with experimental measurements. A broader rationale for invoking this method in a nonlinear dynamics study is available in prior publications.[1,6]

The problem was solved under the following general assumptions: 1) incompressible laminar flow; 2) constant mass density and specific heat, but possible temperature-dependent dynamic viscosity and thermal conductivity; 3) negligible viscous heating; 4) negligible body forces in comparison to viscous forces; and 5) $\Delta \leq \delta$. The last assumption restricts the model to fluids with Prandtl numbers greater than about unity. However, in a related study,[6] results have been shown to remain accurate to within 2% for $Pr > 0.7$.

Conservation Equations and Boundary Conditions

Transient boundary-layer equations for momentum conservation in differential and integral forms, which correspond to the aforementioned assumptions and stagnation flow in Fig. 1, are

$$\frac{\partial u}{\partial t} + u\frac{\partial u}{\partial x} + v\frac{\partial u}{\partial y} = -\frac{1}{\rho}\frac{\partial p}{\partial x} + \frac{\partial}{\partial y}\left(\nu\frac{\partial u}{\partial y}\right) \tag{2}$$

$$\frac{\partial}{\partial t}\int_0^\delta u\,dy - U_\infty\frac{\partial \delta}{\partial t} + \frac{\partial}{\partial x}\int_0^\delta u(u - U_\infty)\,dy + \frac{\partial U_\infty}{\partial x}\int_0^\delta u\,dy = -\frac{1}{\rho}\int_0^\delta \frac{\partial p}{\partial x}dy - \left(\nu\frac{\partial u}{\partial y}\right)\Big|_{y=0} \tag{3}$$

The associated transient boundary-layer equations for energy conservation, in differential and integral forms, are

$$\rho c_p\left(\frac{\partial T}{\partial t} + u\frac{\partial T}{\partial x} + v\frac{\partial T}{\partial y}\right) = \frac{\partial}{\partial y}\left(k\frac{\partial T}{\partial y}\right) \tag{4}$$

$$\frac{\partial}{\partial t}\int_0^\Delta T\,dy - T_\infty\frac{\partial \Delta}{\partial t} + \frac{\partial}{\partial x}\int_0^\Delta u(T - T_\infty)\,dy = -\frac{1}{\rho c_p}\left(k\frac{\partial T}{\partial y}\right)\Big|_{y=0} \tag{5}$$

With reference to the unsteady stagnation flow in Fig. 1, $\delta = \delta(x, t)$, $\Delta = \Delta(x, t)$, $u = u(x, y, t)$, $p = p(x, t)$, $U_\infty = U_\infty(x, t)$, and $T = T(x, y, t)$ in Eqs. (2–5).

The differential forms of the momentum and energy conservation equations [Eqs. (2) and (4)], and physically appropriate matching conditions that must be satisfied by specified expressions for $u(x, y, t)$ and $T(x, y, t)$ give the following:

Surface ($y = 0$)

$$u = 0 \tag{6a}$$

$$v = 0 \tag{6b}$$

$$\frac{\partial u}{\partial t} = 0 \tag{6c}$$

$$0 = -\frac{1}{\rho}\frac{\partial p}{\partial x} + \frac{\partial}{\partial y}\left(\nu\frac{\partial u}{\partial y}\right) \tag{6d}$$

$$T = T_s \tag{7a}$$

$$\frac{\partial T}{\partial t} = \frac{1}{\rho c_p}\frac{\partial}{\partial y}\left(k\frac{\partial T}{\partial y}\right) \tag{7b}$$

Edge of hydrodynamic boundary layer ($y = \delta$)

$$u = U_\infty(x, t) \tag{8a}$$

$$\frac{\partial u}{\partial y} = 0 \tag{8b}$$

$$\frac{\partial^2 u}{\partial y^2} = 0 \tag{8c}$$

Edge of thermal boundary layer ($y = \Delta$)

$$T = T_\infty \tag{9a}$$

$$\frac{\partial T}{\partial y} = 0 \tag{9b}$$

$$\frac{\partial^2 T}{\partial y^2} = 0 \tag{9c}$$

Beyond the hydrodynamic boundary layer ($y > \delta$), $u = U_\infty$, and the flow is governed by the time-dependent Euler's equation below:

$$\frac{\partial U_\infty}{\partial t} + U_\infty \frac{\partial U_\infty}{\partial x} = -\frac{1}{\rho}\frac{\partial p}{\partial x} \tag{10}$$

Since $\partial p/\partial y << \partial p/\partial x$ across the velocity boundary layer, Eq. (10) relates the pressure gradient $\partial p/\partial x$ in Eqs. (2), (3), and (6d) to the freestream velocity U_∞.

Model Formulation

Physically correct and temporally adaptive polynomial profiles of fourth-order were assumed for flow velocity and temperature across the hydrodynamic and thermal boundary layers.[1] Transient effects due to freestream velocity variations are incorporated in the velocity profile by Eqs. (6d), (8a), and (10), and by temporal changes in the thickness of the hydrodynamic boundary layer on which the profile depends explicitly. Similarly, transient effects are incorporated in the temperature profile through the energy balance in the fluid at the impingement surface given by Eq. (7b), and by temporal changes in the thickness of the thermal boundary layer. The influence of the hydrodynamic boundary-layer response on the transient thermal boundary-layer thickness is included via advective terms appearing in the energy conservation equation [Eq. (5)]. When subject to Eqs. (6–10), with all thermophysical properties constant and expressed in dimensionless forms, the appropriate polynomials are given by Eqs. (11) and (12)

$$u_* = \left(2 + \frac{\Lambda\Omega}{6}\right)\eta - \frac{\Lambda\Omega}{2}\eta^2 + \left(\frac{\Lambda\Omega}{2} - 2\right)\eta^3 + \left(1 - \frac{\Lambda\Omega}{6}\right)\eta^4 \tag{11}$$

$$\theta = \theta_s - \left(2\theta_s + \frac{\omega}{3}\right)\beta + \omega\beta^2 + (2\theta_s - \omega)\beta^3 + \left(\frac{\omega}{3} - \theta_s\right)\beta^4 \tag{12}$$

where

$$\Omega = \frac{1}{U_{\infty *}}\frac{\partial U_{\infty *}}{\partial \tau} + \frac{1}{C_*}\frac{\partial U_{\infty *}}{\partial x_*} \tag{13}$$

$$\omega = \Gamma\frac{Pr}{2}\frac{d\theta_s}{d\tau} \tag{14}$$

The properties ρ and c_p are assumed constant throughout the analysis. ν and k, however, are considered to vary linearly with the fluid temperature according to the following relationships:

$$\nu = \nu_f[1 + \alpha_\nu(\theta - 0.5)] \tag{15}$$

$$k = k_f[1 + \alpha_k(\theta - 0.5)] \tag{16}$$

Upon combining Eqs. (3), (10), (11), and (15) and carefully observing functional dependencies, a partial differential equation for the hydrodynamic boundary layer $\delta(x, t)$ results, in which explicit functions of the spatial variable x appear only as products with $\partial\delta/\partial x$. The symmetry in the dividing flow about the stagnation streamline and the associated spatial constancy of the hydrodynamic boundary layer ($\partial\delta/\partial x = 0$) is invoked to remove all such terms. An ordinary differential equation with t as the sole independent variable is thereby obtained, and is given below in terms of a dimensionless hydrodynamic boundary-layer thickness Λ ($=C\delta^2/\nu_f$) and the dimensionless time τ ($=Ct$):

$$\frac{d\Lambda}{d\tau}\frac{1}{20}\left[(\Omega_1 + \Omega_2)\frac{1}{4}\Lambda - 3\right] = -2 + \Psi_1\Lambda - \Psi_2\Lambda^2 - \Psi_3\Lambda^3 - \alpha_\nu(\theta_s - 0.5)\left[2 + \frac{(\Omega_1 + \Omega_2)\Lambda}{6}\right] \tag{17}$$

where

$$\Omega_1 = \frac{1}{U_{\infty *}}\frac{\partial U_{\infty *}}{\partial \tau} \tag{18a}$$

$$\Omega_2 = \frac{1}{C_*}\frac{\partial U_{\infty *}}{\partial x} \tag{18b}$$

$$\Psi_1 = (2/15)\Omega_1 + (116/315)\Omega_2 \tag{19}$$

$$\Psi_2 = (1/120)\Omega_1^2 + (71/3780)\Omega_1\Omega_2 + (79/7560)\Omega_2^2 \tag{20}$$

$$\Psi_3 = (1/4536)(\Omega_1 + \Omega_2)^2\Omega_2 \tag{21}$$

An energy balance at the surface is used to relate the surface temperature to the imposed surface heat flux:

$$q_s = -\left(k\frac{\partial T}{\partial y}\right)\Big|_{y=0} = -\frac{k_f}{\Delta}(T_{s0} - T_\infty) \times [1 + \alpha_k(\theta_s - 0.5)]\frac{\partial\theta}{\partial\beta}\Big|_{\beta=0} \tag{22}$$

The dimensionless temperature gradient $\partial\theta/\partial\beta$ in the fluid is readily determined from Eq. (12). With this result, combined with Eq. (22) and Eq. (16), the transient ordinary differential equation for the dimensionless surface temperature θ_s is readily found and is given by

$$\frac{d\theta_s}{d\tau} = \frac{6}{Pr\Gamma}\left[\frac{q_{s*}\Gamma^{1/2}}{1 + \alpha_k(\theta_s - 0.5)} - 2\theta_s\right] \tag{23}$$

where q_{s*} is defined below:

$$q_{s*} = \frac{q_s}{k_f\sqrt{(C/\nu_f)}(T_{s0} - T_\infty)} \tag{24}$$

With the condition $\partial\Delta/\partial x = 0$ for the thermal boundary layer within the stagnation region, Eqs. (5), (11), (13), and (16) yield the ordinary differential equation for the time-depen-

dent, dimensionless thermal boundary-layer thickness Γ ($=C\Delta^2/\$_f$):

$$\frac{d\Gamma}{d\tau}\left\{4 - \frac{q_{s*}}{[1 + \alpha_k(\theta_s - 0.5)]\theta_s}\Gamma^{1/2}\right\} = \frac{96}{Pr} - \Gamma^{1/2}\frac{28}{Pr}\frac{q_{s*}}{[1 + \alpha_k(\theta_s - 0.5)]\theta_s} - \Gamma^{3/2}f_1(\Lambda, \theta_s) + \Gamma^2 f_2(\Lambda, \theta_s) - \Gamma^{5/2}f_3(\Lambda, \theta_s) - \Gamma^3 f_4(\Lambda, \theta_s) + \Gamma^{7/2}f_5(\Lambda, \theta_s) + \frac{\alpha_k}{Pr}g(\theta_s, \Gamma) \quad (25)$$

where

$$f_1(\Lambda, \theta_s) = 4\Omega_2\Lambda^{-1/2} + \frac{1}{3}\Psi_4\Lambda^{1/2} - \frac{1}{[1 + \alpha_k(\theta_s - 0.5)]\theta_s}\frac{dq_{s*}}{d\tau} \quad (26)$$

$$f_2(\Lambda, \theta_s) = \frac{1}{3}\left\{\frac{8}{7}\Psi_4 + \left(2\Omega_2\Lambda^{-1/2} + \frac{1}{6}\Psi_4\Lambda^{1/2}\right)\frac{q_{s*}}{[1 + \alpha_k(\theta_s - 0.5)]\theta_s}\right\} \quad (27)$$

$$f_3(\Lambda, \theta_s) = \frac{1}{7}\left\{\frac{5}{4}\Psi_4\Lambda^{-1/2} - 5\Omega_2\Lambda^{-3/2} + \frac{1}{2}\Psi_4\frac{q_{s*}}{[1 + \alpha_k(\theta_s - 0.5)]\theta_s}\right\} \quad (28)$$

$$f_4(\Lambda, \theta_s) = \frac{1}{7}\Lambda^{-1/2}\left(\left\{\frac{4}{3}\Lambda^{-1/2} + \frac{q_{s*}}{[1 + \alpha_k(\theta_s - 0.5)]\theta_s}\right\}\Omega_2\Lambda^{-1} - \left\{\frac{2}{9}\Lambda^{-1/2} + \frac{1}{4}\frac{q_{s*}}{[1 + \alpha_k(\theta_s - 0.5)]\theta_s}\right\}\Psi_4\right) \quad (29)$$

$$f_5(\Lambda, \theta_s) = \frac{5}{126}\frac{q_{s*}}{[1 + \alpha_k(\theta_s - 0.5)]\theta_s}\Lambda^{-1}\left(\Omega_2\Lambda^{-1} - \frac{1}{6}\Psi_4\right) \quad (30)$$

$$g(\theta_s, \Gamma) = \frac{q_{s*}\Gamma^{1/2}}{[1 + \alpha_k(\theta_s - 0.5)]\theta_s}\left\{20(\theta_s - 0.5) + \frac{12\theta_s}{1 + \alpha_k(\theta_s - 0.5)} - \frac{6q_{s*}\Gamma^{1/2}}{[1 + \alpha_k(\theta_s - 0.5)]^2}\right\} \quad (31)$$

$$\Psi_4 = (\Omega_1 + \Omega_2)\Omega_2 \quad (32)$$

The convective heat transfer coefficient is obtained from Eq. (12) and Newton's law of cooling:

$$h = \frac{-\left(k\frac{\partial T}{\partial y}\right)\Big|_{y=0}}{T_s - T_\infty} = \frac{-\left(k\frac{\partial \theta}{\partial \beta}\right)\Big|_{\beta=0}}{\theta_s\Delta} \quad (33)$$

With the temperature gradient at the surface obtained from Eq. (12), the Nusselt number Nu_w ($=hw/k_f$) is obtained.

$$Nu_w = w\sqrt{(C/\nu_f)} \times \frac{q_{s*}}{\theta_s} \quad (34)$$

The resulting instantaneous Nusselt number is spatially constant, as expected in the stagnation region. Its time-averaged value is of ultimate interest in many practical situations and, when referenced to the steady-state (nonpulsating) Nusselt number $Nu_* = Nu_w/Nu_{w0}$ is defined as

$$Nu_{*,\text{avg}} = \int_0^{n/f_*} Nu_*\theta_s\, d\tau \Big/ \int_0^{n/f_*} \theta_s\, d\tau \quad (35)$$

Equation (35) is readily derived from an instantaneous energy balance at the surface and Newton's law of cooling. It thereby gives results equivalent to what would be measured experimentally. No influence on heat transfer due to pulsations is indicated when $Nu_{*,\text{avg}} = 1$. Integration was performed over a large number n of pulsation periods $1/f_*$ to ensure accuracy to within the smallest decimal place in all reported values.

Forcing Functions for Freestream Flow and Surface Heat Flux

An important advantage of the present model is that boundary-layer behavior can be predicted for any specified temporal variation in the velocity $U_{\infty*}(x_*, \tau)$ [$=U_\infty/V_{i0}$] in Eq. (8a), or surface heat flux $q_{s*}(\tau)$ in Eq. (24), so long as the variations are piecewise smooth. Since the precise characteristics of temporal flow variations are dependent on specific physical circumstances, the general features of Eq. (1) for steady stagnation flow were assumed to apply so as to obtain forcing functions that converge on the steady flow case as forcing frequencies approach zero. Therefore, transient terms were introduced by assuming that the dimensionless velocity gradient C_* ($=Cw/V_i$) from potential flow theory remains unchanged, and that unsteadiness in the incident velocity $V_i(t)$ (Fig. 1) induces temporal variations in the dimensional velocity gradient C_t [$=C_*V_i(t)/w$]. The influences of the flow pulse characteristics and surface heat flux variations are assessed by analyzing responses to different forcing functions for $U_{\infty*}(x_*, \tau)$ and $q_{s*}(\tau)$.

A general functional form is adopted that can lead to both sinusoidal and ramp-up/ramp-down variations, depending on the values of the parameters ξ_1 and ξ_2. All forcing functions are specified about initial, steady-state values:

$$0 < \tau \le \frac{\xi_1}{f_*}: \quad u_{\infty*}(x_*, \tau) = C_*x_*\left(1 + \varepsilon_1\cos\frac{\pi f_*}{\xi_1}\tau\right) \quad (36a)$$

$$\frac{\xi_1}{f_*} < \tau \le \frac{1}{f_*}: \quad u_{\infty*}(x_*, \tau) = C_*x_*\left[1 - \varepsilon_1\cos\frac{\pi f_*}{1 - \xi_1} \times \left(\tau - \frac{\xi_1}{f_*}\right)\right] \quad (36b)$$

$$0 < \tau \le \frac{\xi_2}{f_{q*}}: \quad q_{s*}(\tau) = q_{s0*}\left(1 + \varepsilon_2\cos\frac{\pi f_{q*}}{\xi_2}\tau\right) \quad (37a)$$

$$\frac{\xi_2}{f_{q*}} < \tau \le \frac{1}{f_{q*}}: \quad q_{s*}(\tau) = q_{s0*}\left[1 - \varepsilon_2\cos\frac{\pi f_{q*}}{1 - \xi_2} \times \left(\tau - \frac{\xi_2}{f_{q*}}\right)\right] \quad (37b)$$

where the initial steady heat flux was obtained from Eq. (23) and is given by

$$q_{s0*} = \frac{2 + \alpha_k}{\sqrt{\Gamma_0}} \quad (38)$$

As can be inferred, ξ is the fraction of the total pulse period for the ramp-down portion of the pulse, and $1 - \xi$ is the remaining portion of the ramp-up portion. Pulses profiles with different values for ξ are illustrated in Fig. 1b. When $\xi = 0.5$, a pure sine-wave pulse is obtained. As $\xi \to 0$ (or 1), the periodic pulse has a very steep ramp-down (or ramp-up). Other ramp-up/ramp-down pulses are obtained with intermediate values for ξ. The ramp-up/ramp-down pulses, when modeled piecewise with sine functions in this manner, contain continuous higher derivatives, and thereby represent physically plausible pulse waveforms.

In many practical situations, the heat transfer surface may be electrically heated with alternating current. Thereby, in addition to the aforementioned forcing function, a sine-squared function is defined in Eq. (39) for the ensuing surface heat flux variations. The parameter ε_3 displaces the sine-squared curve upward in order to represent the thermal inertia of the electrically heated body:

$$q_{s*}(\tau) = q_{s0*}\{\varepsilon_3 + 2(1 - \varepsilon_3)\sin^2[2\pi f_{q*}\tau + (\pi/4)]\} \quad (39)$$

It is important to note that $0 \leq \varepsilon_i \leq 1$ for $i = 1, 2, 3$ in the expressions above so as to avoid flow and heat reversals for which the model is not applicable.

Solution Methodology and Model Verification

Steady-state (nonpulsating) values Λ_0, Γ_0, and q_{s0*} were determined from Eqs. (17), (23), and (25) with all time-derivatives set to 0 and $\theta_s = \theta_{s0} = 1$. The secant method[7] was used to solve the resulting nonlinear equations to within a convergence tolerance 10^{-6}. For the time-dependent solutions, Runge-Kutta algorithms were implemented to obtain numerical solutions to the three ordinary, nonlinear differential equations [Eqs. (17), (23), and (25)] for Λ, Γ, and θ_s. Variable dimensionless time steps were incorporated in the algorithms to reduce computational time, since calculations sometimes extended over several thousand periods of the forcing functions in order to illustrate the nonlinear dynamic response. Beginning time steps were selected as small fractions of the unforced response time (see below) or of the forcing function period. Maximum time steps were successively halved until differences in successive computations were within a tolerance of 10^{-6}. In addition, both fourth-order and fifth-order Runge-Kutta algorithms were used to ensure algorithm-independence in the calculated results. Power spectral densities were determined from results calculated with constant time steps equal to the smallest time step encountered in the respective solution with the variable time step approach.

Representing the velocity and temperature profiles with temporally adaptive fourth-order polynomials [Eqs. (11) and (12)] restricted the numerical solutions to conditions for which the profiles remained physically realistic. For the velocity field, the restricting criteria are expressed by the inequalities $|\Lambda\Omega| < 12$; $\Lambda\Omega \neq 6$. The temperature profiles are restricted to the cases when $|\omega| < 6\theta_s$; $\omega \neq 3\theta_s$. The criteria above, if satisfied, preclude the occurrence of imaginary roots and corresponding unrealistic maxima and minima in the temporally adaptive profiles. In general, the model eventually breaks down under a combination of high amplitude and high-frequency fluctuations in the forcing functions. Stability of solutions was also investigated by employing the linearization theorem technique, because it requires the least computational effort for very complex nonlinear equations.[8] Stable behavior for a boundary layer was considered to be any condition where the boundary-layer response approaches a limit cycle, and is thereby periodic.

The model was verified by comparison under steady-state conditions to known analytical solutions, and under transient conditions to experimental results for stagnation flows about cylinders and spheres. Values of Λ_0 and Γ_0 were identical to those reported by Zumbrunnen[6] for the constant-property case, and calculated Nusselt numbers were determined to be within 1–2.3% of those obtained from the similarity solutions for a constant-property flow past a wedge.[25] Sheriff and Zumbrunnen[9] reported significant reductions in time-averaged stagnation line Nusselt numbers for impinging pulsating planar water jets that agree with the theoretical predictions of the present model to within 2%.

Results and Discussion

Equations (17), (23), and (25) constitute a nonautonomous system of three, coupled, nonlinear, ordinary differential equations that govern the dynamical responses of the hydrodynamic and thermal boundary layers, in terms of the variables Λ and Γ, and of the surface temperature, in terms of θ_s. Although the governing energy equation is linear in temperature for the constant property case, Eq. (23) is nonlinear due to imbedded nonlinearities that emerge upon employing the energy equation to obtain governing equations for Γ. (That is, the energy equation is nonlinear with respect to the thermal boundary-layer thickness.) When taken together with the forcing functions for incident flow velocity and surface heat flux given by Eqs. (35–40), solutions in terms of τ ($= Ct$) are dependent on the parameters Pr, C_*, ε_1, ε_2, f_*, f_{q*}, ξ_1, and ξ_2. The responses are strongly influenced in dimensional terms by C ($= C_* V_{i0}/w$). Freestream velocity gradients are smaller in stagnation flows with larger characteristic dimensions, and the hydrodynamic and thermal boundary-layer responses are thereby less rapid for impinging jets with larger widths or for cylinders with larger diameters in a crossflow. Values of C_* for cylinders and planar jets are given in Ref. 6 and may be used to convert the dimensionless results presented in this study to dimensional values for specific applications. Steady-state values of Λ and Γ (i.e., Λ_0 and Γ_0) depend on the coefficients α_ν and α_k in Eqs. (15) and (16), as inspection of Eqs. (17) and (23) indicates. For the constant property case, $\alpha_\nu = \alpha_k = 0$, and Λ_0 and Γ_0 are uniquely defined for a specified fluid.

Before considering forced responses, it is of interest to discuss the responses of Eqs. (17) and (25) with no external forcing to clarify the simplest boundary-layer behavior. For the unforced responses, an initial surface temperature equal to unity ($\theta_s = 1$), steady incident flow ($\varepsilon_1 = 0$), and steady surface heat flux ($\varepsilon_2 = 0$) were specified and the boundary-layer thicknesses were initially taken to be zero. With constant properties, the thermal boundary-layer thicknesses approached steady-state values in an asymptotic fashion to within 1% at τ equal to 9 and 15 for Prandtl numbers of 0.7 and 15, respectively. The hydrodynamic boundary layer approached its steady-state value to within 1% when $\tau = 3$. As boundary-layer development proceeded, the corresponding Nusselt numbers approached steady-state values to within 1% at dimensionless times equal to 6 and 9 for Prandtl numbers of 0.7 and 15, respectively. With temperature-dependent kinematic viscosity [Eq. (15)], the response of the hydrodynamic boundary layer was delayed up to 2 units in terms of τ for $-0.2 < \alpha_\nu < 0.05$, which includes temperature dependencies representative of air and water. A temperature dependence for thermal conductivity had little affect on the unforced thermal boundary layer and Nusselt number responses within the range $0.05 < \alpha_k < 2.5$, with steady-state values attained at nearly the same time-intervals as in the constant property case. The dimensionless times given above give some indication of the responsiveness of the boundary layers. However, since the governing system is highly nonlinear, no characteristic time interval can be precisely identified. Results suggest that temperature-dependent properties do not strongly influence time scales.

The influence of Prandtl number with constant properties $\alpha_\nu = 0$ and $\alpha_k = 0$, and constant surface heat flux $\varepsilon_2 = 0$, is shown in Fig. 2 in the presence of sinusoidal flow pulsations, $\xi_1 = 0.5$ in Eq. (36). Λ undergoes nonsinusoidal oscillations, reflecting the nonlinear content of Eq. (17). Its response is

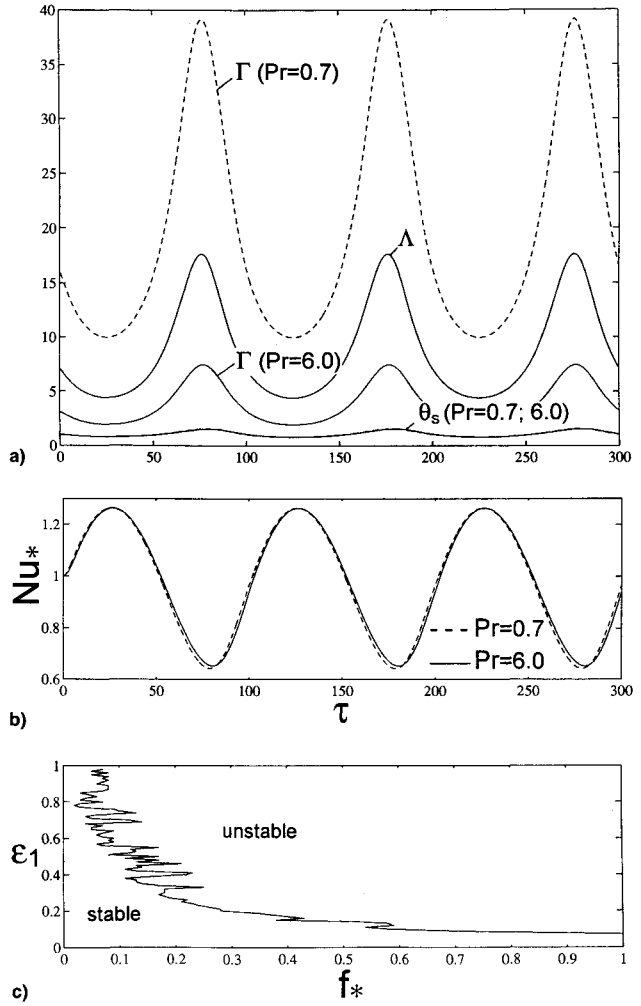

Fig. 2 Influence of Prandtl number on response for constant surface heat flux ($\varepsilon_2 = 0$), and sinusoidal flow pulsations with $f_* = 0.01$, ($\varepsilon_1 = 0.6$), and constant properties ($\alpha_\nu = \alpha_k = 0$): a) dimensionless boundary-layer thicknesses and surface temperature, b) Nusselt number, and c) solution stability map for $Pr = 6.0$ and $\varepsilon_2 = \alpha_\nu = \alpha_k = 0$.

not affected by Prandtl number, since the momentum and energy equations are uncoupled when properties do not depend on temperature. Γ increases with decreasing Prandtl number, reflecting a greater thermal diffusivity. As is the case for Λ, the responses are nonsinusoidal. Time-averaged Nusselt numbers and the dimensionless surface temperatures decrease slightly, but remain within 1% of steady-state values. Responses for the ramp-up/ramp-down flow pulsations [$\xi_1 \neq 0.5$ in Eq. (36)] were found to be qualitatively similar.

A stability analysis was applied to Eq. (17) governing the dimensionless hydrodynamic boundary-layer thickness for the constant property case. Stable behavior was considered to be any condition where the boundary-layer response approaches a limit cycle, and is thereby periodic. Stability was assessed by invoking the linearization theorem[8] and calculating a time-averaged eigenvalue. Responses were deemed stable if the time-averaged eigenvalue was negative.[10] Results are summarized in Fig. 2c, wherein the boundary between stable and unstable behavior is complex. The investigation was performed with a resolution of 0.01 in both f_* and ε_1. Since Eq. (17) is uncoupled in the constant property case to Eqs. (23) and (25), chaotic behavior for Λ cannot arise and the unstable situation refers to unbounded solutions for Λ corresponding to a positive time-averaged eigenvalue. Under these conditions, Λ grows uncontrollably and a breakdown in boundary-layer behavior might be anticipated in physical systems. The unstable region in Fig. 2c may therefore suggest conditions where interesting behavior may arise in experimental studies of pulsating flows.

The dynamic responses with temperature-dependent properties, sinusoidal flow pulsations, and constant surface heat flux ($\varepsilon_2 = 0$) are shown in Fig. 3. The kinematic viscosity and thermal conductivity depend on temperature according to Eqs. (15) and (16). Values for the viscosity coefficient α_ν [Eq. (15)], and the thermal conductivity coefficient α_k [Eq. (16)] are characteristic of water at ambient temperature. Consideration of such transport property variations is important as the momentum and energy equations become coupled. As in Fig. 2, sinusoidal flow pulsations lead to nonsinusoidal responses. Since viscosity decreases with temperature, the response for $\alpha_\nu = -0.14$ falls below that for $\alpha_\nu = 0$. The thermal boundary-layer response in terms of Γ for $\alpha_k = 0.50$ falls above the constant property response since thermal conductivity increases with temperature. The instantaneous Nusselt number exhibits slightly larger variations for the variable property case. For sinusoidal flow pulsations and the particular values assigned to the parameters in Fig. 3, the time-averaged values of Λ, Γ, and θ_s change by -18, 20, and -2.3%, respectively, compared to the constant-property case ($\alpha_\nu = \alpha_k = 0$). The Nusselt number, scaled to its steady-state value and time-averaged according to Eq. (35), decreases below steady-state values in both cases. The convective heat transfer is reduced, with a greater reduction occurring in the constant property case (-7.4%) in comparison to the temperature-dependent case (-6.7%). When the magnitudes of α_ν and α_k are greater by a factor of 10, the time-averaged Nusselt number decreases by 1.2%. Hence, with stronger temperature-dependency, the resulting decrease in Nusselt number is less pronounced.

The flow pulsation waveform can be significantly modified by varying the coefficient ξ_1 in Eq. (36) as demonstrated in Fig. 1b. Figure 4 presents the influence of flow pulse waveform on the system dynamics and is representative of all responses for $f_* < 0.05$. Higher dimensionless frequencies could not be considered since aforementioned model stability cri-

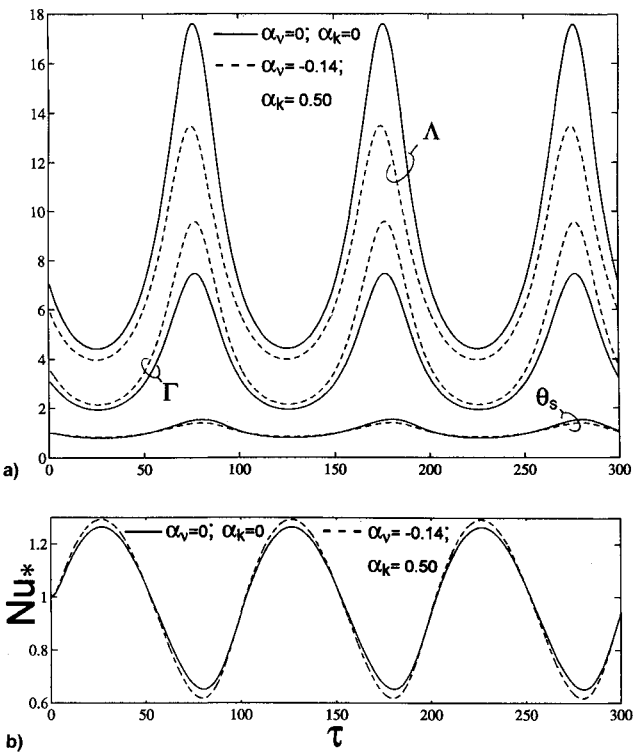

Fig. 3 Influence of temperature-dependent properties on the response for a constant surface heat flux ($\varepsilon_2 = 0$), and sinusoidal flow pulsations ($\xi_1 = 0.5$) with $f_* = 0.01$, $\varepsilon_1 = 0.6$, and $Pr = 6$: a) dimensionless boundary-layer thicknesses and surface temperature and b) Nusselt number.

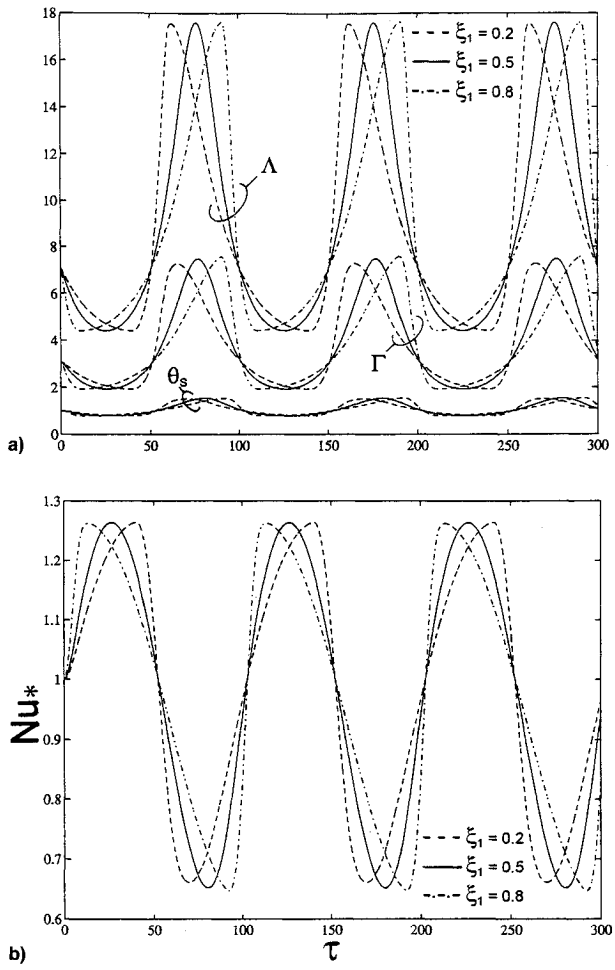

Fig. 4 Influence of flow pulsation profile with $f_* = 0.01$, $\varepsilon_1 = 0.6$, $Pr = 6$, a constant surface heat flux ($\varepsilon_2 = 0$), and constant properties $\alpha_\nu = \alpha_k = 0$: a) dimensionless boundary-layer thicknesses and surface temperature and b) Nusselt number.

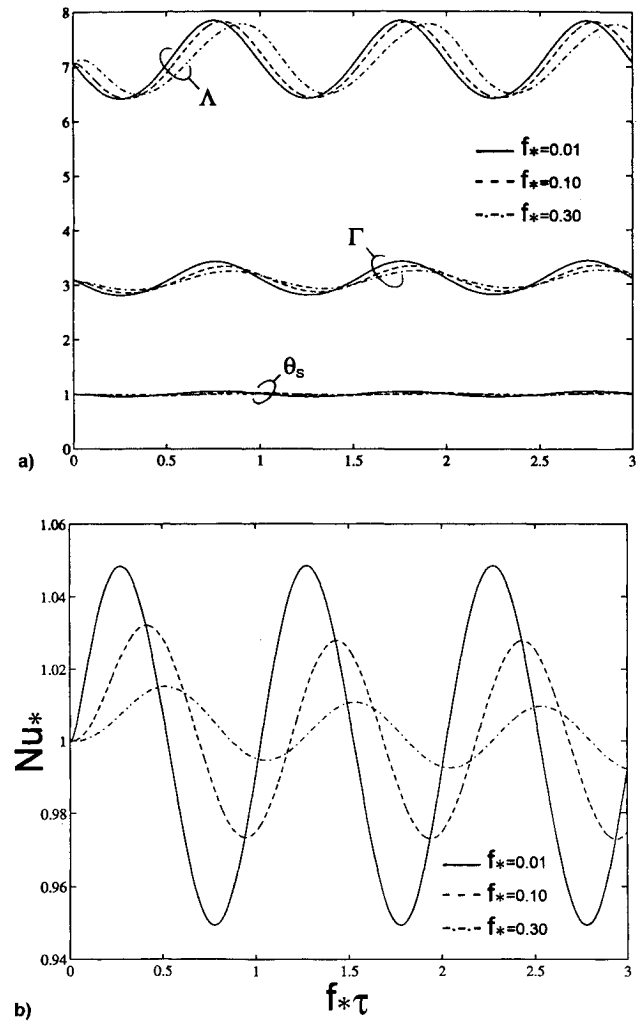

Fig. 5 Influence of flow pulsation frequency f_* for sinusoidal flow pulsations ($\xi_1 = 0.5$) with $\varepsilon_1 = 0.6$, $Pr = 6$, a constant surface heat flux ($\varepsilon_2 = 0$), and constant properties ($\alpha_\nu = \alpha_k = 0$): a) dimensionless boundary-layer thicknesses and surface temperature and b) Nusselt number.

teria were not satisfied. Flow pulsations with a steep decrease and slow increase ($\xi_1 < 0.5$), with a slow decrease and steep increase ($\xi_1 > 0.5$), and a pure-sine waveform ($\xi_1 = 0.5$), are compared. The responses indicate that, despite differences in the instantaneous behaviors, the time-averaged responses of the boundary layers and Nusselt number remain within 0.5% of each other. Thus, enhancing heat transfer by careful selection of pulse shape does not appear to be feasible for $f_* < 0.05$. However, it is useful to note that since time-averaged Nusselt numbers are insensitive to pulse shape, results obtained with a particular pulse waveform can be applied generally.

In order to deduce the influence of pulsation frequency and pulsation amplitude, each was treated separately as a parameter in Figs. 5 and 6, and results are summarized in Fig. 7 in terms of corresponding time-averaged Nusselt numbers. A constant surface heat flux ($\varepsilon_2 = 0$), and constant properties ($\alpha_\nu = 0$ and $\alpha_k = 0$) are imposed. Instantaneous responses in Fig. 5 vary with the flow pulsation frequency where the pulse magnitude ε_1 is identical in all cases. Mancuso and Diller[11] concluded that the heat transfer is flow-driven when the surface temperature is constant, and therefore a periodic unsteadiness in the flow is reflected in an unsteadiness in the heat transfer at the surface. However, for the conditions considered here, it is obvious from Fig. 5 that pulsation frequency, as well as pulse magnitude, can influence instantaneous heat transfer. Over a large frequency range in Fig. 5, a positive increasing phase shift is produced in the periodic responses of each variable at increasing frequencies. Departures from steady-state (e.g., $\tau = 0$) values become smaller at higher frequencies. Gradually, asymptotic values are reached, since the system response is too sluggish in comparison to the very rapid perturbations, as suggested by the unforced time responses discussed earlier. At low frequencies, the instantaneous Nusselt number has a phase angle of 180 deg compared to the dynamics of the boundary-layer thicknesses and the surface temperature. For example, Nusselt number has a maximum when Γ reaches a minimum, which was expected since the boundary layer represents a thermal resistance. An inspection of Eq. (34) also suggests an inverse dependency relationship between Nusselt number and surface temperature. Results indicate that this phase angle exceeds 180 deg with increasing frequencies. Gorla et al.[12] also reported a phase lag in heat transfer compared to freestream fluctuations. The amplitude and phase angle of the fluctuating component of heat transfer decreased and increased, respectively, with a dimensionless frequency parameter. Time-averaged values for all dependent variables in Fig. 5 remain within 1% of corresponding steady-state values. In addition, time-averaged values were found to remain within 1% of steady-state values for $0.1 < \varepsilon_1 < 0.6$.

The influence of flow pulse magnitude ε_1 is depicted in Fig. 6 for a constant surface heat flux ($\varepsilon_2 = 0$), and constant properties ($\alpha_\nu = 0$ and $\alpha_k = 0$), as in Fig. 5. Responses exhibit larger deviations from the initial steady-state values with increasing ε_1. Notably, the time-averaged boundary-layer thicknesses increase dramatically, and time-averaged Nusselt num-

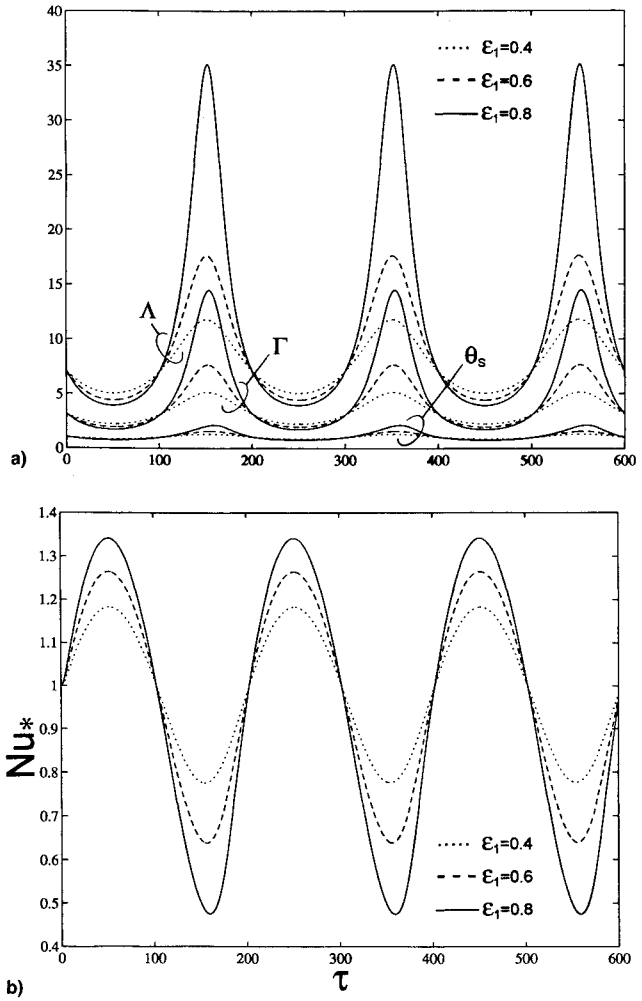

Fig. 6 Influence of flow pulsation amplitude ε_1 for sinusoidal flow pulsations ($\xi_1 = 0.5$) with $f_* = 0.005$, $Pr = 6$, a constant surface heat flux ($\varepsilon_2 = 0$), and constant properties ($\alpha_\nu = \alpha_k = 0$): a) dimensionless boundary-layer thicknesses and surface temperature and b) Nusselt number.

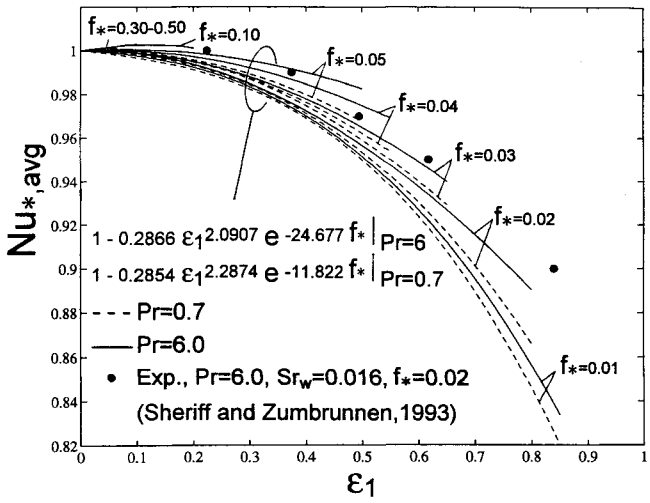

Fig. 7 Influence of Prandtl number and flow pulsation amplitude and frequency on time-averaged Nusselt number for constant properties ($\alpha_\nu = \alpha_k = 0$), and constant surface heat flux ($\varepsilon_2 = 0$).

ber decreases [Eq. (34)] as a consequence. The decrease in time-averaged Nusselt number relative to steady-state reaches 16% for $\varepsilon_1 = 0.8$.

Figure 7 summarizes the influences of fluid Prandtl number and flow pulsation frequency and amplitude on time-averaged Nusselt number when a constant surface heat flux and constant properties are imposed. Results are expressed in terms of time-averaged Nusselt number scaled to its steady-state value. Consequently, any significant influence on heat transfer from the surface is marked by a departure of $Nu_{*,\text{avg}}$ from unity. Results indicate that the time-averaged Nusselt number decreases monotonically with increasing flow pulse amplitude ε_1 when the dimensionless pulsation frequency f_* is less than about 0.1. The decreases are most pronounced at lower dimensionless frequencies and Prandtl numbers. When $f_* = 0.10$, the scaled Nusselt number has a maximum at $\varepsilon_1 = 0.12$ slightly greater than unity. Model stability criteria that were discussed previously limited pulsation amplitudes ε_1 below 0.10 for $0.30 < f_* < 0.50$, in which case predicted Nusselt numbers are shown to increase slightly. It should be noted that the present model can be used to assess the influence of small freestream turbulence since stagnation region boundary layers remain essentially laminar for small turbulence intensities due to a favorable pressure gradient. Thus, the high-frequency/small-amplitude flow pulsations mimic small eddies due to an incident turbulence. Results suggest that such eddies can enhance heat transfer due to nonlinear dynamics effects alone. Model results are represented succinctly by the equations indicated on Fig. 7 to within 0.3%. These equations are applicable to the ranges for ε_1 indicated in the figure, and for $0.01 < f_* < 0.1$.

Model-predicted time-averaged Nusselt numbers in Fig. 7 are in excellent agreement with values determined experimentally by Sheriff and Zumbrunnen[9] for a pulsating planar water jet incident on a constant heat flux surface with $f_* = 0.02$ and $Re_w = 6.85 \times 10^3$. Both the theoretical and experimental results indicate a significant decrease in Nusselt number with increasing flow pulsation amplitude. Experimentally determined Nusselt numbers exceed theoretical values with $f_* = 0.02$ by less than 2%. Moreover, experimentally determined reductions were insensitive to the jet Reynolds number Re_w as predicted theoretically by the model of this study. Reductions in time-averaged Nusselt numbers may be of practical significance when it is desirable to suppress convective heat transfer from a hot surrounding fluid, as is the case when gas turbine blades are exposed to a periodic flow of hot combustion gases as they pass fixed nozzles.

In Figs. 2–7, a steady surface heat flux was considered in order to focus on the effect of flow pulsations alone. However, cases where temporal variations in the surface heat flux are produced can be of practical interest. For example, when heat is produced due to dissipative losses in a resistive element passing an alternating current, the surface heat flux may be given according to Ohm's law by a sine-squared relationship as in Eq. (39). Figure 8 displays the system dynamics when a sinusoidal flow pulsation is coupled with a surface heat flux pulsation of similar frequency, but of sine-squared-type. The fluid viscosity and thermal conductivity are considered temperature-dependent. Therefore, the higher frequency heat flux fluctuations are reflected in the time history of the hydrodynamic boundary-layer thickness via surface temperature variations that influence the fluid viscosity. Time-averaged values of the boundary-layer thicknesses do not deviate from their corresponding steady-state values at $\tau = 0$. However, $Nu_{*,\text{avg}}$ increases by 0.9% and are accompanied by decreases in θ_s of similar magnitude. The time-histories in Fig. 8 were found to be nonchaotic and to have a period of 29 cycles referenced to f_{q*}.

For other combinations of flow and heat flux pulse characteristics, the responses may become very complex, especially when the fluid properties are considered temperature-dependent. For chaotic behavior to occur, a governing system of at least two coupled, ordinary differential equations for the nonautonomous case (i.e., with external forcing functions) must include nonlinear terms in at least one dependent variable.[13] Hence, the present model may be considered a candidate for generating chaotic solutions. A complex dynamical

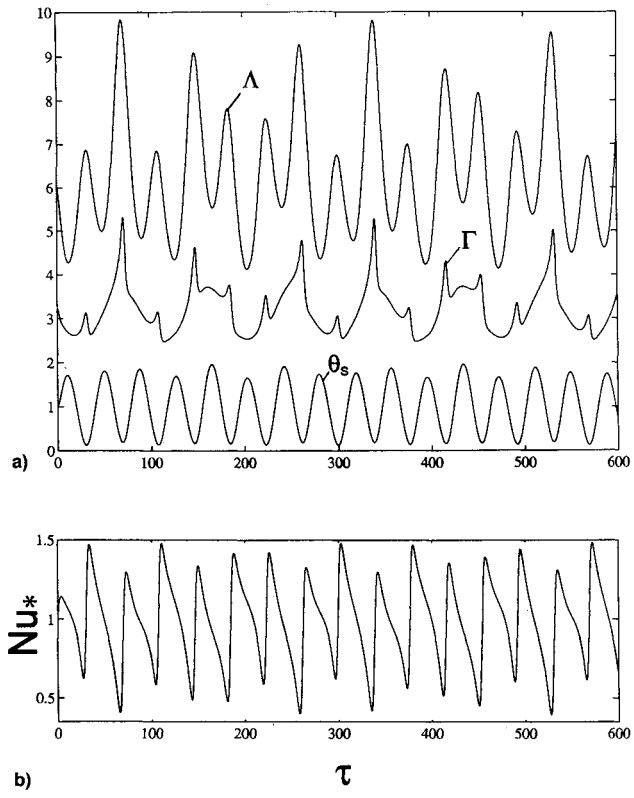

Fig. 8 Response due to sinusoidal flow pulsations ($\xi_1 = 0.5$), and sine-squared surface heat flux variations with $f_* = 0.011$, $\varepsilon_1 = 0.20$, $f_{q*} = 0.013$, $\varepsilon_3 = 0.10$, $Pr = 6$, $\alpha_\nu = -0.14$, and $\alpha_k = 0.05$: a) dimensionless boundary-layer thicknesses and surface temperature and b) Nusselt number.

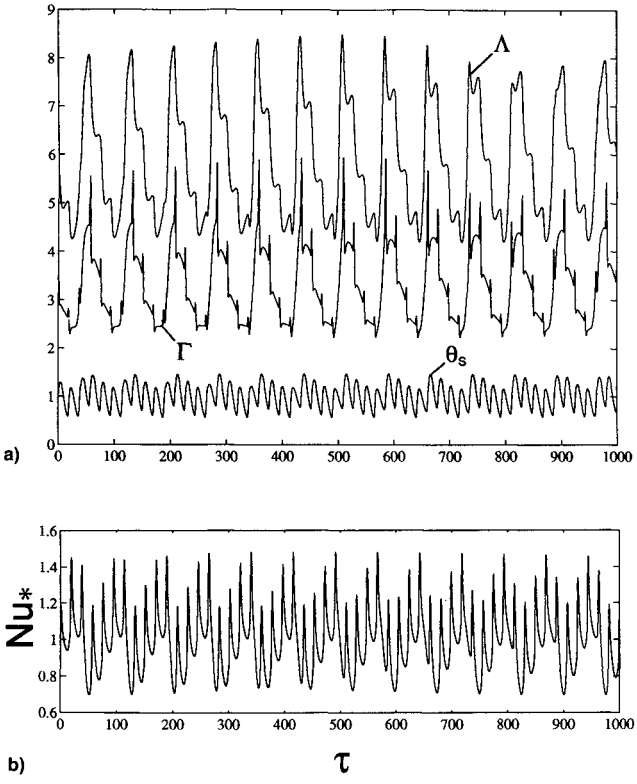

Fig. 9 Response due to simultaneous ramp-up/ramp-down variations in incident flow velocity and surface heat flux with $f_* = 0.013$, $\varepsilon_1 = 0.30$, $f_{q*} = 0.053$, $\varepsilon_2 = 0.40$, $\xi_1 = 0.2$, $\xi_2 = 0.8$, $Pr = 6$, $\alpha_\nu = -0.10$, and $\alpha_k = 0.05$: a) dimensionless boundary-layer thicknesses and surface temperature and b) Nusselt number.

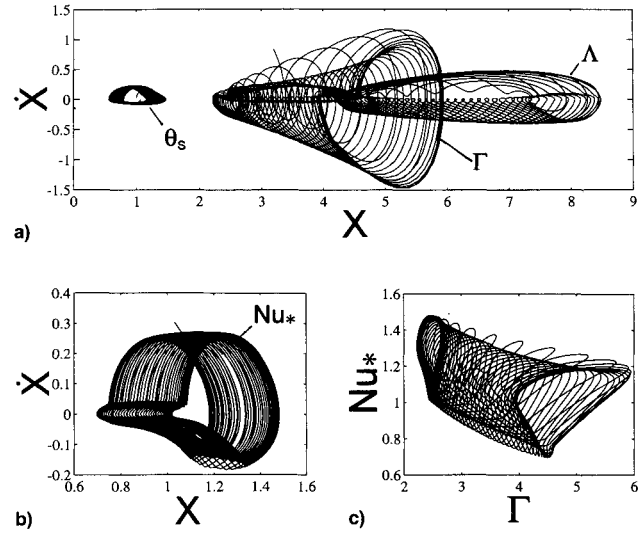

Fig. 10 Phase portraits for the responses of Fig. 9: a) dimensionless boundary-layer thicknesses and surface temperature, b) Nusselt number, and c) Nusselt number vs thermal boundary-layer thickness.

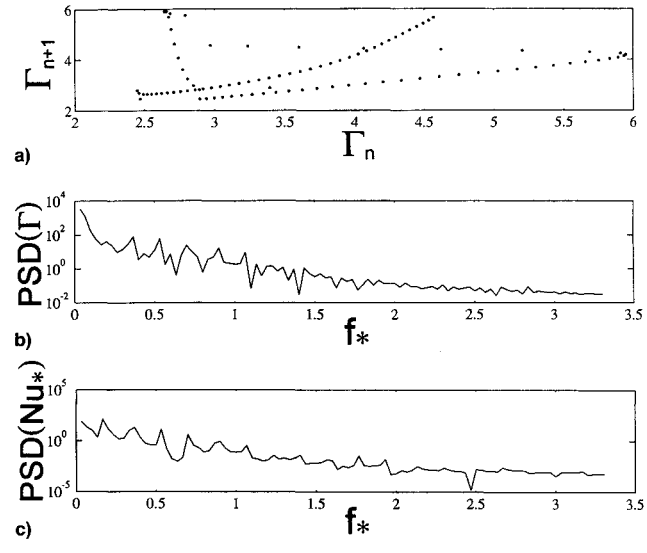

Fig. 11 Characterizations of the responses in Fig. 9: a) Poincaré map of the thermal boundary-layer thickness, b) Fourier spectrum of the thermal boundary-layer thickness, and c) Fourier spectrum of Nusselt number.

response is presented in Figs. 9–11 for a single case where both surface heat flux and incident freestream velocity follow ramp-up/ramp-down waveforms, and where properties depend on temperature. Specifically, the flow pulsation follows a steep ramp-down and a slow ramp-up variation, while the heat flux has a slow decrease followed by a rapid increase. The boundary-layer dynamics in Fig. 9 are profoundly distorted in shape, and the time averages Λ and Γ relative to steady-state values increase by 4 and 6%, respectively. Instantaneous Nusselt numbers also vary in a complex manner and yield a time-averaged value [Eq. (35)] 2% lower than the steady-state value. Owing to the complexity of these responses, tools specific to nonlinear dynamical system analysis[14,15] will be utilized next in order to clarify them further. However, it is obvious that the interaction between a time-dependent incident flow and a time-dependent heat flux can yield very erratic thermal transport conditions, even when the time-dependencies in the flow and heat flux are relatively simple.

Phase portraits of the responses of Fig. 9 are given in Fig. 10. All responses have a complex torus structure as expected in any doubly forced nonlinear system. Since two incommensurate frequencies are imposed, it is expected that the trajectories will have a quasiperiodic nature and will appear to "move" on the torus surface along unique paths. The breakup of the quasiperiodic torus structure is one possible route to chaotic behavior that can arise as a system parameter is varied.[14] A Poincaré section through the torus at the zero-derivative level in Fig. 10 preserves one point for each distinct loop (or trajectory), and associates it with a characteristic frequency. A typical multiperiodic response yields a finite number of points on a Poincaré map, a quasiperiodic response has all points lying on a closed curve on the Poincaré map, and a chaotic response yields an unbounded number of points that may form a fractal pattern. The Poincaré map presented in Fig. 11a for the thermal boundary-layer dynamics was based on 200 cycles corresponding to the higher frequency f_{q*}. A period in terms of f_{q*} equal to 94 cycles was revealed and reflects an increased complexity in the system response.

The Fourier spectra of the thermal boundary-layer thickness and Nusselt number are presented in Figs. 11b and 11c. Both spectra reveal an irregular distribution of peaks over the frequency range and do not exhibit clear spikes at the forcing frequencies. Such broad frequency spectra are characteristic of chaotic responses. However, the largest Lyapunov exponent[14] for the conditions of Figs. 9–11 was determined to equal −0.3248. Since a negative Lyapunov exponent signifies an insensitivity of responses to initial conditions, the very complex responses of Fig. 9 are nonchaotic and can be categorized as quasiperiodic in consideration of the suggested loops in the Poincaré map of Fig. 11a.

The very complex responses of Fig. 9, although shown to be nonchaotic, point to the possibility that other combinations of model parameters might yield chaotic behavior. Such chaotic behavior can be potentially beneficial if corresponding time-averaged thermal transport characteristics are altered appreciably. To this end, the theoretical model of this study can treat accurately a diversity of situations and succumb to standard diagnostic techniques for characterizing nonlinear dynamical behavior. A systematic but partial search was performed to assess the influence of parameters on the system's largest Lyapunov exponent. For a sinusoidal flow pulsation and constant surface heat flux with $\varepsilon_1 = 0.2$ and $0.01 < f_* < 0.1$, or $f_* = 0.1$ and $0.2 < \varepsilon_1 < 0.3$, the largest Lyapunov exponent became less negative as frequency or amplitude was increased. However, the negative Lyapunov exponents indicated that nonchaotic behavior prevails for sinusoidal pulse waveforms and this range of parameters. As previously mentioned, the solution stability map of Fig. 2c suggests other conditions where interesting behavior might arise.

Conclusions

The dependence of convective heat transfer to a pulsating stagnation flow was investigated theoretically under the conditions of incompressible flow and symmetry in the incident flow about a stagnation streamline. High-frequency/low-amplitude pulsations in an incident flow can lead to small (<1%) increases in time-averaged Nusselt numbers relative to steady-state conditions. This result suggests that incident turbulence can enhance heat transfer due to nonlinear dynamics effects alone. Low-frequency/high-amplitude pulsations in an incident flow can yield reductions in time-averaged Nusselt number. Reductions of up to 16% were predicted and are in good agreement with recent experimental results. Such reductions might have practical application in reducing heat transfer to gas turbine blades. Although instantaneous responses differed, time-averaged Nusselt numbers varied by less than 1% for various pulse shapes in the incident flow velocity for dimensionless frequencies $f_* < 0.05$. Higher dimensionless frequencies were not considered since model stability criteria could not be satisfied. Temperature-dependent properties led to more complex behavior in transport quantities, but did not influence appreciably the corresponding time-averaged values. Temporal variations in the surface heat flux, when combined with flow pulsations, can give rise to very complex dynamical behavior due to competing influences on the hydrodynamic and thermal boundary layers. In consideration of the highly nonlinear system of governing equations and the number of parameters, the possibility that chaotic responses might occur in actual applications cannot be as yet excluded, although none were encountered in this study.

Acknowledgment

Support for this work was provided by the National Science Foundation of the United States under Grant MSS-9253640.

References

[1]Mladin, E. C., and Zumbrunnen, D. A., "Nonlinear Dynamics of Laminar Boundary Layers in Pulsatile Stagnation Flows," *Journal of Thermophysics and Heat Transfer*, Vol. 8, No. 3, 1994, pp. 514–523.

[2]Schlichting, H., *Boundary-Layer Theory*, 7th ed., McGraw-Hill, New York, 1979, pp. 95–99, 206–217.

[3]Inada, S., Miyasaka, Y., and Izumi, R., "A Study of the Laminar Flow Heat Transfer Between a Two-Dimensional Water Jet and a Flat Surface with Constant Heat Flux," *Bulletin of the Japan Society of Mechanical Engineers*, Vol. 24, No. 196, 1981, pp. 1803–1810.

[4]Kuethe, A. M., and Schetzer, J. D., *Foundation of Aerodynamics*, Wiley, New York, 1959.

[5]Zumbrunnen, D. A., Incropera, F. P., and Viskanta, R., "A Laminar Boundary Layer Model of Heat Transfer Due to a Nonuniform Planar Jet Impinging on a Moving Plate," *Wärme- und Stoffübertragung*, Vol. 27, No. 1, 1992, pp. 311–319.

[6]Zumbrunnen, D. A., "Transient Convective Heat Transfer in Planar Stagnation Flows with Time-Varying Surface Heat Flux and Temperature," *Journal of Heat Transfer*, Vol. 114, No. 1, 1992, pp. 85–93.

[7]Gerald, C. F., *Applied Numerical Analysis*, Addison-Wesley, Reading, MA, 1987, pp. 11–13.

[8]Jeffries, C. D., *Mathematical Modeling in Ecology: A Workbook for Students*, Birkhauser Publication, Boston, MA, 1992, pp. 36–68.

[9]Sheriff, H., and Zumbrunnen, D. A., "Effect of Flow Pulsations on the Cooling Effectiveness of an Impinging Planar Water Jet," *Journal of Heat Transfer* (to be published).

[10]Hale, J. K., and Koçak, H., *Dynamics and Bifurcations*, Springer-Verlag, New York, 1991.

[11]Mancuso, T., and Diller, T. E., "Time-Resolved Heat Flux Measurements in Unsteady Flow," *Proceedings of the 1991 National Heat Transfer Conference*, 1991, pp. 67–74 (HTD-Vol. 179).

[12]Gorla, R. S. R., Jankowski, F., and Textor, D., "Thermal Response of a Periodic Boundary Layer Near an Axisymmetric Stagnation Point on a Circular Cylinder," *International Journal of Heat and Fluid Flow*, Vol. 9, No. 4, 1988, pp. 427–430.

[13]Parker, T. S., and Chua, L. O., *Practical Numerical Algorithms for Chaotic Systems*, Springer-Verlag, New York, 1989, pp. 1–56.

[14]Moon, F., *Chaotic Vibrations*, Wiley, New York, 1987.

[15]Drazin, P. G., *Nonlinear Systems*, Cambridge Univ. Press, New York, 1992, pp. 261–277.

[16]Van der Hegge Zijen, B. G., "Heat Transfer from Horizontal Cylinders to a Turbulent Air Flow," *Applied Scientific Research*, Vol. 7(A), 1958, pp. 205–223.

[17]Sreenivasan, K., and Ramachandran, A., "Effect of Vibration on Heat Transfer from a Horizontal Cylinder to a Normal Air Stream," *International Journal of Heat and Mass Transfer*, Vol. 3, No. 1, 1961, pp. 60–67.

[18]Nevins, R. G., and Ball, H. D., "Heat Transfer Between a Flat Plate and a Pulsating Impinging Jet," *Proceedings of the 1961 National Heat Transfer Conference* (Boulder, CO), Vol. 60, 1961, pp. 510–516.

[19]Kasza, K. E., "Thermal Response Characteristics of Unsteady Stagnation Point Flows: A New Approach," *International Journal of Heat and Mass Transfer*, Vol. 18, No. 2, 1975, pp. 329–331.

[20]Saxena, U. C., and Laird, A. D. K., "Heat Transfer from a Cylinder Oscillating in a Cross Flow," *Journal of Heat Transfer*, Vol.

100, No. 4, 1978, pp. 684–689.

[21]Andraka, C. E., and Diller, T. E., "Heat-Transfer Distribution Around a Cylinder in Pulsating Crossflow," *Journal of Engineering for Gas Turbines and Power*, Vol. 107, No. 4, 1985, pp. 976–982.

[22]Gorla, R. S. R., Jankowski, F., and Textor, D., "Periodic Boundary Layer Near an Axisymmetric Stagnation Point on a Circular Cylinder," *International Journal of Heat and Fluid Flow*, Vol. 9, No. 4, 1988, pp. 421–426.

[23]Eibeck, P. A., Keller, J. O., Bramlette, T. T., and Sailor, D. J., "Pulse Combustion: Impinging Jet Heat Transfer Enhancement," *Proceedings of the International Symposium on Pulsating Combustion*, Vol. 2, 1991, pp. 1–25.

[24]Zumbrunnen, D. A., and Aziz, M., "Convective Heat Transfer Enhancement Due to Intermittency in an Impinging Jet," *Journal of Heat Transfer*, Vol. 115, No. 1, 1993, pp. 91–98.

[25]Evans, H. L., "Mass Transfer Through Laminar Boundary Layers. 7. Further Similar Solutions to the B-Equation for the Case B = 0," *International Journal of Heat and Mass Transfer*, Vol. 5, No. 1, 1962, pp. 35–37.